Determination of Heat Capacity of Yucca Mountain Stratigraphic Layers

Teklu Hadgu, Clinton Lum and James E. Bean

Sandia National Laboratories

Corresponding Author: Teklu Hadgu
Sandia National Laboratories
P. O. Box 5800, MS0776
Albuquerque, NM 87185-0776
Phone: (505)844-7945, email: thadgu@sandia.gov

ABSTRACT

The heat generated from the radioactive waste to be placed in the proposed geologic repository at Yucca Mountain, Nevada, will affect the thermal-hydrology of the Yucca Mountain stratigraphic layers. In order to assess the effect of the movement of repository heat into the fractured rocks accurate determination of thermodynamic and hydraulic properties is important. Heat capacity is one of the properties that are required to evaluate energy storage in the fractured rock. Rock-grain heat capacity, the subject of this study, is the heat capacity of the solid part of the rock. Yucca Mountain consists of alternating lithostratigraphic units of welded and non-welded ash-flow tuff, mainly rhyolitic in composition and displaying varying degrees of vitrification and alteration. A number of methods exist that can be used to evaluate heat capacity of the stratigraphic layers that consist of different compositions. In this study, the mineral summation method has been used to quantify the heat capacity of the stratigraphic layers based on Kopp's rule. The mineral summation method is an addition of the weighted heat capacity of each mineral found in a specific layer. For this study the weighting was done based on the mass percentage of each mineral in the layer. The method utilized a mineralogic map of the rocks at the Yucca Mountain repository site. The Calico Hills formation and adjacent bedded tuff layers display a bimodal mineral distribution of vitric and zeolitic zones with differing mineralogies. Based on this bimodal distribution in zeolite abundance, the boundary between the vitric and zeolitic zones was selected to be 15% zeolitic abundance. Thus, based on the zeolite abundance, subdivisions have been introduced to these layers into "vitric" and "zeolitic" zones. Heat capacity values have been calculated for these layers both as "layer average" and "zone average". The heat capacity determination method presented in this report did not account for spatial variability in the horizontal direction within each layer.

1. INTRODUCTION

Yucca Mountain, Nevada has been designated as the site of our nation's proposed high-level radioactive waste repository and the U. S. Department of Energy (DOE) has been approved to apply to the U. S. Nuclear Regulatory Commission (NRC) for a license to construct a repository. A diagram depicting the Yucca Mountain repository Site is shown in Figure 1. Heat transfer and energy storage in the Yucca Mountain Project (YMP) host rock is an important aspect of repository waste emplacement. Canisters containing radioactive waste are to be emplaced in tunnels drilled 250-500 m below the ground surface. After waste emplacement, decaying heat is transferred from the canisters to the host rock by a combination of heat transfer mechanisms. In order to assess the performance of the repository, studies of heat transfer and fluid flow processes in the emplacement drifts as well as in the host rock are required. Modeling of heat flow in the host rock requires accurate representation of thermal properties of the specific rock materials at Yucca Mountain. One of the properties of interest is the heat capacity of the rocks which is used to evaluate energy storage.

Heat capacity is a key thermodynamic property. For the purpose of this report, it is defined as the amount of energy required to raise the temperature of a unit mass of material by one degree. It has the units of J/(g•K). For solids isobaric heat capacity, C_p, is virtually independent of pressure but a strong function of temperature. The heat capacity of a rock mass consists of heat capacity of rock grains and heat capacity and latent heat of fluids in the rock. This report deals with the rock grain heat capacity only. The term specific heat is often used synonymously with heat capacity; however, the latter term is used throughout this report.

Several methods can be used to estimate heat capacity of rock grains. Nimick and Connolly (1991, pp. 5-11) report three different methods for heat capacity estimation: oxide summation, mineral summation and fictive-oxide mineral-component method.

- The oxide summation method uses oxide abundance data and heat capacity of oxides to evaluate heat capacity of rock grains.
- The mineral summation method uses mineral abundance data and heat capacity of minerals to evaluate rock grain heat capacity.
- The fictive-oxide mineral-component method proposed by Robinson and Haas (1983) as a more accurate method for estimating heat capacity of solids. This method requires detailed information on composition and structure of mineral species, and very accurate weight fraction measurements.

For this study the oxide summation method was not used due to lack of relevant complete and up-to-date oxide data. The fictive-oxide mineral-component method was also not used because of unavailability of required information. Instead, the mineral summation method was selected due to the availability of relevant mineral abundance and mineral heat capacity data. The method uses the sum of the heat capacities of minerals in a layer weighted by their abundance. Here abundance refers to mass fraction of a mineral in the layer. Information on the stratigraphic layers and mineral abundance data are found in the Mineralogic Model (MM3.0) report (BSC 2004a, Section 6.2.3). Figure 2 shows a schematic stratigraphic column with relative thicknesses of the units.

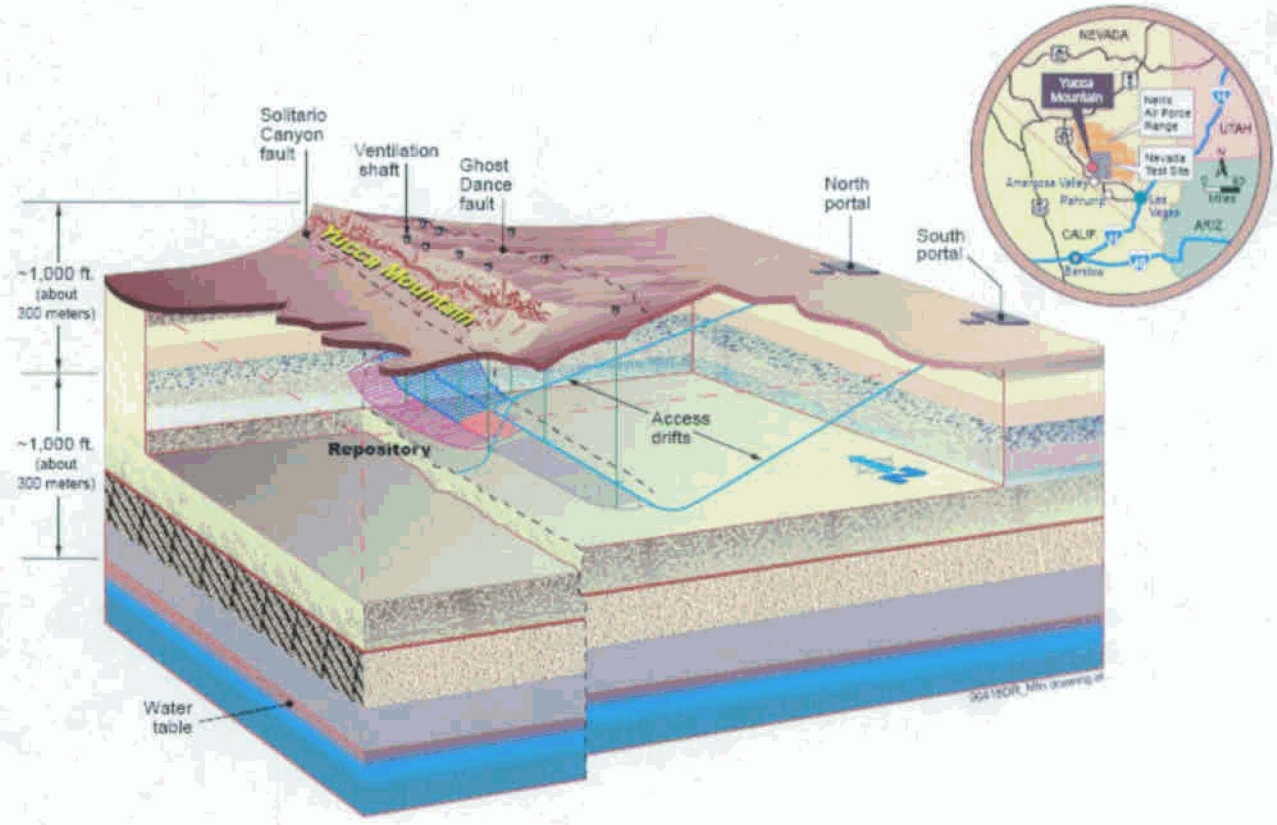

Figure 1: Schematic Diagram of the Yucca Mountain Repository Site

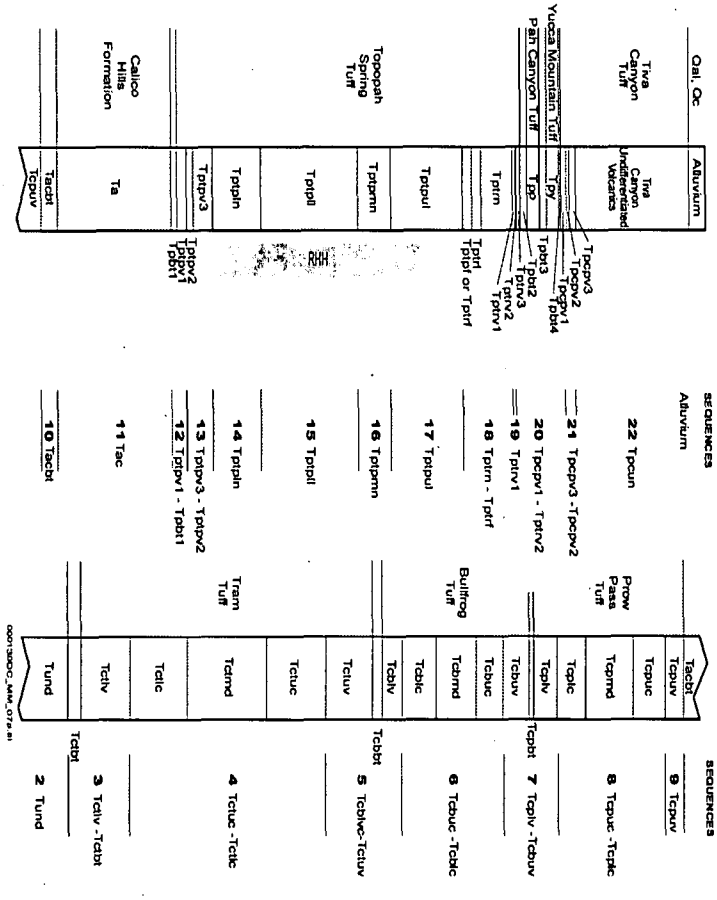

Figure 2: Schematic Stratigraphic Column with relative Thicknesses of Units (Excluding Units Between Qual or QC and Tpc, and Paleozoic units)

(From Mineralogic Model (MM3.0) report (BSC 2004a, Figure 6-4)

2. MINERAL ABUNDANCE OF MINERAL GROUPS

The heat capacity evaluation uses mineralogy defined in the Mineralogic Model (MM3.0) report (BSC, 2004a, Section 6.2.3). The mineralogic model incorporates mineralogic data from 24 boreholes and provides mineralogic information for each stratigraphic unit. The model defines ten mineral groups shown in Table 1.

Table 1. Mineral groups defined in the Mineralogic Model (BSC 2004a)

Number	Mineral Group	Member Mineral	Mineral Formula
1	smectite and illite	smectite	$Ca_{.025}Na_{.1}K_{.2}Fe^{++}{}_{.5}Fe^{+++}{}_{.2}Mg_{1.15}Al_{1.25}Si_{3.5}H_2O_{12}$
		illite	$K_{.6}Mg_{.25}Al_{2.3}Si_{3.5}O_{10}(OH)_2$
2	sorptive zeolites	clinoptilolite	$Na_{.954}K_{.543}Ca_{.761}Mg_{.124}Sr_{.036}Ba_{062}Mn_{002}Al_{3.45}Fe_{.017}Si_{14.533}O_{29.066}\cdot 17.856H_2O$
		mordenite	$Ca_{.2895}Na_{.361}Al_{.94}Si_{5.06}O_{12}\cdot 3.468H_2O$
		chabazite	$K_{0.6}Na_{0.2}Ca_{1.5}Al_{3.8}Si_{8.2}O_{24}\cdot 10.0H_2O$
		erionite	$K_{1.5}Na_{.9}Ca_{.9}Al_{4.2}Si_{13.8}O_{36}\cdot 13.0H_2O$
		stellerite	$Ca_{2.0}Al_{4.0}Si_{14}O_{36}\cdot 14.0H_2O$
3	tridymite		SiO_2
4	cristobalite and opal-CT	Cristobalite	SiO_2
		Opal-CT	SiO_2
5	quartz		SiO_2
6	feldspars		$KAlSi_3O_8$
7	volcanic glass		see Appendix A
8	nonsorptive zeolite (analcime)		$Na_{0.96}Al_{0.96}Si_{2.04}O_6\cdot 1.0H_2O$
9	mica		$KAl_3Si_3O_{10}(OH)_2$
10	calcite		$CaCO_3$

The mineral abundance data used in this study was developed based on data generated using the x-ray powder diffraction (XRD) technique. The mineral abundances are divided into 22 sequences and 26 layers (Figure 2 shows the sequences, with the exception of Sequence 1). The 22 sequences were defined to keep the mineralogic model simpler, and to accurately define zeolitic, vitric and repository host units. For 25 of the 26 layers, the software EARTHVISION (Dynamic Graphics, 2000) was used to calculate the average and standard deviation mineral abundance values for the ten mineral groups for each stratigraphic layer. The results of the calculation are documented in the Mineralogic Model (MM3.0) report (BSC, 2004a). In the present report mineral abundances for selected layers are provided in Tables 2 to 4. Units Tpcpv1, Tptbt4, Tpy, Tpbt3, Tpp, Tpb2, Tptrv3, and Tptrv2 (Sequence 20 of the mineralogic model) are included in Table 1 as a single unit, the PTn.

Examining the mineral abundances for all layers, the minerals with significant abundances are feldspars, sorptive zeolites, silica polymorphs (i.e. tridymite, cristobalite, opal-CT and quartz), and volcanic glasses. Feldspars are found in all layers and are the most abundant mineral, except in Sequences 11 to 13 (Figure 2, layers in the Calico Hills formation and above). The sorptive zeolites group represents clinoptilolites, heulandite, mordenite, chabazite, erionite and stellerite. They are grouped due to their capacity to absorb water, which is an important factor in radionuclide transport. Sorptive zeolites are significant in the Calico Hills formation layers and the layers immediately above and below it. The most abundant sorptive zeolites are clinoptilolite and mordenite. Heulandite is a fairly common mineral, but its XRD determined abundance was

combined with clinoptilolite because the two minerals have the same crystal structure (BSC 2004a, p. 6-21). Silica polymorphs can be found in all layers with significant abundances. The primary silica polymorphs are cristobalite and quartz, while tridymite abundances are generally much smaller. In general tridymite has higher abundance in the upper layers, from the Calico Hills formation and above. In contrast, quartz is the dominant silica polymorph in layers below the Calico Hills formation. Volcanic glass is abundant in the non-welded layers (bedded tuffs). The non-welded layers are the PTn and surrounding layers, and Calico Hills formation and surrounding layers.

In terms of their abundances, the remaining mineral groups (smectite, analcime, mica, and calcite) are much less significant: most do not exceed 10 percent. The only exception is smectite, which exceeds 10 percent in a few layers. In general, analcime, mica, and calcite have very low abundances (less than 2 percent), the only exception is analcime which exceeds 5 percent in Sequence 2 (Figure 2, Layer Tund). Analcime is a zeolite with low water sorption capacity. Thus, it is termed as a non-sorptive zeolite to distinguish it from the rest of the zeolites discussed in this report.

Layers of the Calico Hills formation are characterized as vitric or zeolitic (Flint 1998, page 29.). This bimodal composition also characterizes the bedded tuff layers adjacent to the Calico Hills formation (Tptpv3 – Tptpv2, Tptpv1 – Tpbt1, and Tacbt). The compositional character of these layers is illustrated in the Mineralogical Model (MM3.0) report (BSC 2004a, Figures 6-5 to 6-16, 6-19, and 6-20). To determine the mineralogic composition of the vitric and zeolitic zones of these layers, the geographic boundary between the zones needs to be established. To determine the location of the zeolitic-vitric boundary, histograms of zeolite abundance were plotted for each layer. All histogram plots displayed a bimodal distribution of low and high zeolite abundance. Based on this bimodal distribution in zeolite abundance the boundary between the vitric and zeolitic zones in these layers was selected to be 15% zeolitic abundance. The EARTHVISION software (Dynamic Graphics, 2000) was then used to calculate the mineral abundance for the 10 groups in the vitric and zeolitic zones of the layers. The regions with 15% zeolite abundance and above were characterized as "zeolitic". Regions with less than 15% zeolitic abundance were characterized as "vitric". The mineral abundances of the "zeolitic" and "vitric" zones are presented in Tables 3 and 4, respectively.

Table 2. Mineral Abundance for Selected Layers of the Mineralogic Model (MM3.0) Report (BSC 2004a)

Unit	Smectite - Illite average	Smetite – Illite standard deviation	Zeolite average	Zeolite standard deviation	Tridymite average	Tridymite standard deviation	Cristobalite – Opal Ct average	Cristobalite – Opal CT standard deviation	Quartz average	Quartz standard deviation
Tpc_un (Sequence 22)	1.20	0.61	0.15	0.26	0.51	3.34	27.59	5.26	0.93	0.37
PTn (Sequence 20)	12.13	4.93	1.68	2.51	2.10	2.09	8.07	5.51	1.30	0.69
Tptpll (Sequence 15)	2.48	2.13	0.23	0.28	2.09	1.33	14.54	6.75	19.94	5.93
Tac4 (Sequence 11)	1.16	0.53	39.11	27.32	0.02	0.08	13.98	6.02	5.50	2.20
Tcplv – Tcbuv (Sequence 7)	4.87	4.28	47.64	12.26	0.06	0.14	9.54	2.94	8.83	6.18
Tcbuc – Tcblc (Sequence 6)	2.01	1.30	0.22	0.37	0.20	0.32	4.72	4.47	28.16	6.49
Unit	**Feldspars average**	**Feldspars standard deviation**	**Volcanic Glass average**	**Volcanic Glass standard deviation**	**Analcime average**	**Analcime standard deviation**	**Mica average**	**Mica standard deviation**	**Calcite average**	**Calcite standard deviation**
Tpc_un (Sequence 22)	62.45	8.24	8.71	0.24	0.00	0.00	0.47	0.90	0.44	0.55
PTn (Sequence 20)	24.81	13.00	41.11	18.33	0.00	0.00	0.94	0.50	0.85	1.33
Tptpll (Sequence 15)	59.36	6.76	0.00	0.00	0.00	0.00	0.21	0.11	0.07	0.10
Tac4 (Sequence 11)	22.48	10.13	20.80	24.86	0.00	0.00	0.40	0.32	0.00	0.00
Tcplv – Tcbuv (Sequence 7)	25.37	3.46	2.67	3.69	2.29	4.08	0.42	0.37	0.00	0.00
Tcbuc – Tcblc (Sequence 6)	60.45	5.13	0.17	0.28	0.00	0.00	3.04	2.22	0.16	0.26

Table 3. Mineral Abundance in the Zeolitic Zones of Layer Tac4 of the Mineralogic Model (MM3.0) Report (BSC 2004a)

Unit	Smectite - Illite average	Smetite - Illite standard deviation	Zeolite average	Zeolite standard deviation	Tridymite average	Tridymite standard deviation	Cristobalite – Opal CT average	Cristobalite – Opal CT standard deviation	Quartz average	Quartz standard deviation
Tac4	1.33	0.42	54.18	16.79	0.00	0.02	17.42	3.25	4.52	1.47
Unit	**Feldspars average**	**Feldspars standard deviation**	**Volcanic Glass average**	**Volcanic Glass standard deviation**	**Analcime average**	**Analcime standard deviation**	**Mica average**	**Mica standard deviation**	**Calcite average**	**Calcite standard deviation**
Tac4	20.58	11.26	5.86	10.14	0.00	0.00	0.34	0.34	0.00	0.00

Table 4. Mineral Abundance in the Vitric Zones of Layer Tac4 of the Mineralogic Model (MM3.0) Report (BSC 2004a)

Unit	Smectite - Illite average	Smetite - Illite standard deviation	Zeolite average	Zeolite standard deviation	Tridymite average	Tridymite standard deviation	Cristobalite – Opal CT average	Cristobalite – Opal CT standard deviation	Quartz average	Quartz standard deviation
Tac4	0.76	0.55	3.02	3.33	0.05	0.14	5.75	1.29	7.83	1.86
Unit	**Feldspars average**	**Feldspars standard deviation**	**Volcanic Glass average**	**Volcanic Glass standard deviation**	**Analcime average**	**Analcime standard deviation**	**Mica average**	**Mica standard deviation**	**Calcite average**	**Calcite standard deviation**
Tac4	27.02	3.98	56.56	6.16	0.00	0.00	0.55	0.17	0.00	0.00

3. HEAT CAPACITY OF THE MINERAL GROUPS

To calculate the heat capacity of each layer, the heat capacities of the ten mineral groups must be determined. The heat capacity of minerals can be determined by using a variety of calorimetric techniques. The measured data is usually represented using empirical equations ("curve fit") or tables of heat capacity versus temperature. To retain accuracy of measurement when analytical methods (i.e. equations) are used, proper representation of the data is important. To represent heat capacity as a function of temperature different investigators have used a number of forms of equations. The units of heat capacity of these equations vary according to the definition of heat capacity used based on mass, volume or molar. For this study the various units were converted to J/(g•K). Berman and Brown (1985) looked at numerous sources of heat capacity equations. Many of these equations (e.g. Robie et al., 1979) are applicable to heat capacity representation within the calorimetric measurement temperature range. Berman and Brown (1985, Equation 7) presented the following heat capacity equation for minerals:

$$C_p = k_0 + k_1 T^{-0.5} + k_2 T^{-2} + k_3 T^{-3} \quad (1)$$

The coefficients k_0, k_1, k_2 and k_3 are determined so that Equation (1) best fits experimental measurements of heat capacity for each mineral. Berman and Brown (1985, p. 168) claim that Equation (1) reproduces calorimetric data within the estimated precision of the measurements. The absolute deviation of Equation (1) from heat capacity data is less than one percent (Berman and Brown 1985, Table 3, pp. 170-174). Chipera et al. (1995, p. 569) used Equation (1) to fit heat capacity data of zeolites from different sources. The authors used the resulting equations to represent heat capacity of Yucca Mountain zeolites.

Robie et al. (1979, p. 2) provided heat capacity data using Equation (2) to fit experimental mineral heat capacity data:

$$C_p = A_1 + A_2 T + A_3 T^{-2} + A_4 T^{-0.5} + A_5 T^2 \quad (2)$$

Robie et al. (1979, pp. 2 and 218) give lower and upper limits of temperature for each mineral, and caution that Equation (2) should not be extrapolated beyond the upper limit. The upper temperature limits are usually above or within acceptable range for this study (325 °C), and thus extrapolations to higher temperatures would not be necessary. For this work the heat capacity and formula weight data for tridymite (Robie et al., 1979, p. 218) and the heat capacity and formula weight data for silica glasses (Robie and Hemingway, 1995, pp. 31 to 40, 50, and 58 to 66) have been used.

For analcime, Johnson et al. (1982, p. 744, Equation 4) used the following equation:

$$C_p = A_1 + A_2 T + A_3 T^2 + A_4 T^3 \quad (3)$$

In BSC (2004c, Data Tracking Numbers: MO0009THRMODYN.001 and MO0302SPATHDYN.001) the heat capacity equations given here by Equations (1) to (6) are used. Equations (4) to (6) are truncated forms of Equation (2).

$$C_p = A_1 + A_2T + A_3T^{-2} \quad (4)$$

$$C_p = A_1 + A_2T + A_3T^{2} \quad (5)$$

$$C_p = A_1 + A_2T + A_3T^{-0.5} + A_4T^{-2} \quad (6)$$

A listing of the heat capacity equations used for each mineral, together with other relevant information, is provided in BSC (2004b, Appendix A). A summary of the heat capacity sources used for the ten mineral groups is given in Appendix A of this report.

Silica oxide polymorphs such as tridymite and cristobalite exhibit phase transformations at different temperatures (see Thompson and Wennemer, 1979, pp. 1018 to1025). Thompson and Wennemer report major tridymite transitions at 390 K (116.85 °C) and 436 K (162.85 °C), and a cristobalite transition at 535 K (261.85 °C). These transitions absorb heat and, therefore, increase the heat capacity of the minerals as a function of temperature (Nimick and Connolly, 1991, p. 20). Nimick and Connolly (1991) calculated an estimated increase in heat capacity due to the transitions, and show that the heat capacity increase for tridymite is much lower than that of cristobalite. As shown in Thompson and Wennemer (1979, Figures 1 and 2), the transitions cause relatively narrow spikes in the heat capacity-temperature plot. As discussed in Appendix A of this report, the equation for tridymite given by Robie et al. (1979) has a lower limit of 117 °C, which is also the lower temperature transition of Thompson and Wennemer (1979). The equation does not show the upper temperature transition of Thompson and Wennemer (1979). Thompson and Wennemer (1979, p.1022) report the α-to-β transformation for cristobalite (α: 298 to 523 K, and β: 523 to 2000 K) at 523 K (249.85 °C).

In BSC (2004c, Data Tracking Number: MO0009THERMODYN.001) separate heat capacity equations for α and β cristobalite are given, with temperature limits of 726.85 °C and 1726.85 °C, respectively. Neither of these equations includes the heat capacity spike at transition. For this study, a decision was made to use the equation for α cristobalite because it covers most of the temperatures of interest. Also, for heat capacity values averaged over a temperature range the effect of the phase-transformation heat capacity spikes is minimal.

The heat capacity values for the individual mineral species primarily depend on chemical composition. For mineral species that are combined into mineral groups, and that share a common structure and composition, their heat capacity behavior will also be similar. For example, smectite and illite in Group1 have very similar heat capacity values. To simplify the rock-grain heat capacity calculation the heat capacity equation of smectite was used to represent both smectite and illite. The group heat capacity of sorptive zeolites (Group 2) was obtained by averaging the heat capacities of the individual members at specified temperatures. Therefore, simplifications that select, average, or combine heat capacity values for mineral groups are justifiable.

Figure 3 shows heat capacity plots for the ten mineral groups as a function of temperature, in the temperature range of 25 °C to 325 °C. The group heat capacities were calculated using the equations presented in BSC (2004b, Appendix A). The figure shows a nearly linear relationship between heat capacity and temperature, except at lower temperatures. The figure also shows that

most of the mineral groups display similar heat capacity-temperature functions except for the sorptive zeolites and analcime (non-sorptive zeolite), which have higher heat capacities. Among the sorptive zeolites clinoptilolite has the highest heat capacity values. Feldspar shows the highest temperature variations of heat capacity values in the 25 °C to 325 °C range, with values varying by up to 60 %. Sorptive zeolites and analcime also show significant temperature variations in the same temperature range. Smectite and volcanic glasses show the lowest temperature variations in the same temperature range, with about 30 % change in values.

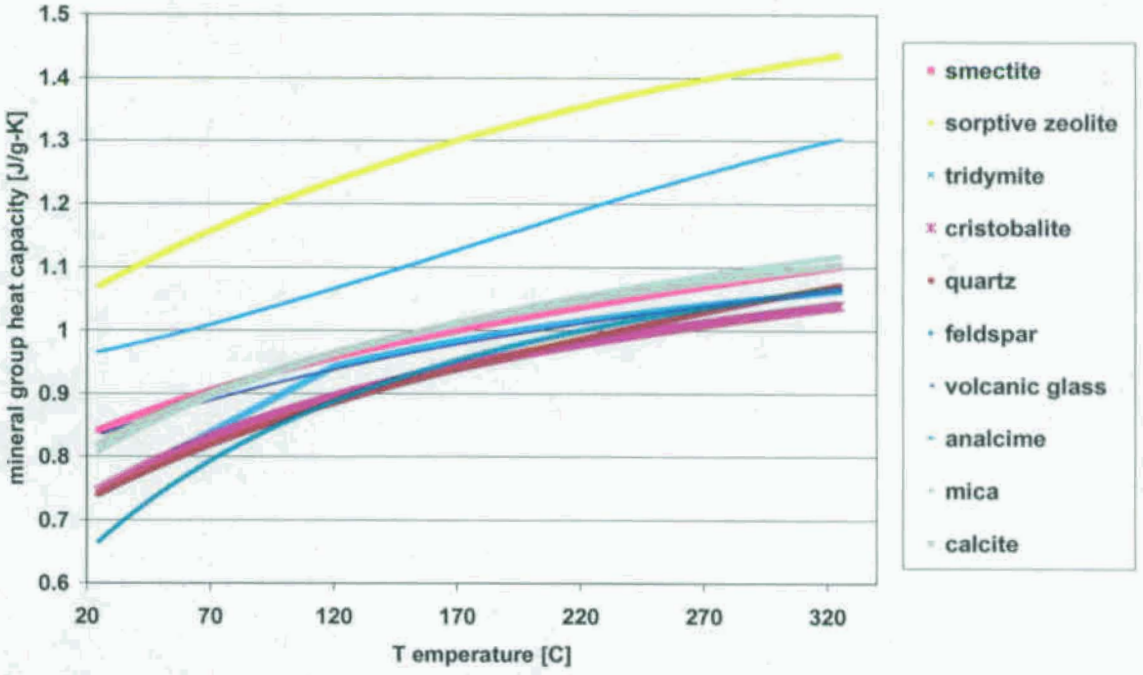

Figure 3. Average Mineral Group Heat Capacity (refer to Table 1 and Appendix A for chemical composition of the mineral groups)

4 ROCK-GRAIN HEAT CAPACITY OF STRATIGRAPHIC LAYERS

As stated in Section 1, for this study the mineral summation method was used to estimate heat capacity of mineral composites in each Yucca Mountain stratigraphic unit. The summation was done according to Kopp's rule (Nimick and Connolly, 1991, p. 6):

$$C_{p_{eff}} = \sum_{j}^{n} x_j C_{p_j} \qquad (7)$$

where x_j and C_{pj} are mineral abundance (mass fraction) and heat capacity of mineral j in J/(g•K), and C_{peff} is the effective heat capacity [J/(g•K)]. According to Kopp's rule the heat capacity of component j in the composite is the same as that of mineral j on its own (Berryman, 1995, p. 218). This has been an acceptable method to estimate heat capacities of most substances (Robinson and Haas, 1983; Nimick and Connolly, 1991). Berryman (1995, p. 219) and others

show that there is a temperature dependent correction to Kopp's rule but the correction is small at low temperatures (considered < 500 °C). Thus, Berryman implies that Kopp's rule is acceptable for use at lower temperatures, the temperature conditions that are of interest to this study.

The rock-grain heat capacity for each mineralogic model stratigraphic unit was calculated using Kopp's rule given by Equation (7), with the mineral abundance data described in Section 2, and the mineral heat capacity data given in BSC (2004b, Appendix A). Calculation results for all stratigraphic layers have been documented in BSC (2004b). Results of the calculations for selected stratigraphic layers representing each formation (See Figure 2) are shown in Figures 4 to 6. The plots show average rock-grain heat capacity as a function of temperature for temperatures in the range of 25 °C to 325 °C. Figure 4 represents average rock-grain heat capacity for selected layers. The heat capacity of the Calico Hills layer (Tac4) was obtained by averaging the heat capacities over zeolitic and vitric regions. Figure 5 shows average rock-grain heat capacity curves for the selected Calico Hills layer (Tac4) representing individual separate average heat capacities of the zeolitic and vitric zones, together with an average heat capacity for the entire layer. Figure 6 shows the average and standard deviation rock-grain heat capacity for layer Tptpll, which is a repository host unit. The standard deviation represents uncertainty due to mineral abundance. The statistical method used to estimate the average and standard deviations of the rock-grain heat capacities is given below.

4.1 Statistical Methods Used to Estimate the Average and Standard Deviation of the Rock-Grain Heat Capacity

The equations used to estimate the average and standard deviations of the rock-grain heat capacities are given below. These statistical measures were developed following the principles outlined in Bulmer (1979, pp. 71 to 73). The calculated average and standard deviations are the result of propagating uncertainties in the mineral abundance and mineral heat capacity through Kopp's rule. Uncertainties due to mineral heat capacity measurement are very low and are ignored in this study. Thus, heat capacity uncertainties that are considered in this study are due to averaging of heat capacity over a certain temperature range. If no averaging over temperature is involved, the statistical analysis considers uncertainties in mineral abundance only. The following analysis starts with the general case of determining the combined standard deviation as a result of uncertainties of both mineral abundance and mineral heat capacity. The analysis is then simplified for the case where no temperature averaging of mineral heat capacity is done.

Equation (8) denotes the jth mineral's contribution to the rock-grain heat capacity (i.e., the product of mineral abundance, x_j, expressed as a weight fraction; and mineral heat capacity, C_{pj}) by P_j:

$$P_j = x_j \cdot C_{pj} \tag{8}$$

With this substitution, Equation (7) becomes:

$$C_{p,g} = \sum_{j=1}^{j=n} x_j \cdot C_{pj} = \sum_{j=1}^{j=n} P_j \tag{9}$$

The expected (or average) value of $C_{p,g}$ over a specified temperature range, denoted can be written as the sum of the expected values of the individual mineral contributions where j =1 to n and n is the number of mineral components.

$$E[C_{p,g}] = \sum_{j=1}^{j=n} E[P_j] \tag{10}$$

Treating x_j and C_{pj} as independent random variables (i.e., the abundance of the mineral should not be dependent on the mineral's heat capacity), the expected value of the jth mineral's contribution to the rock-grain heat capacity may be written as

$$E[P_j] = E[x_j] \cdot E[C_{pj}] \tag{11}$$

$E[x_j]$ is the expected value of the mineral abundance x_j of mineral j in a particular lithostratigraphic layer. The variability of C_{pj} is due to the temperature dependence of the heat capacity of individual minerals expressed by Equations (1) to (6). $E[C_{pj}]$ is the expected value of the heat capacity C_{pj} over a specified temperature range. The variability of C_{pj} is due to the temperature independence of the heat capacity of individual minerals expressed by Equations (1) to (6). Combining Equation (10) and Equation (11) gives the equation for the expected or average value of the rock-grain heat capacity in terms of mineral abundance expressed in terms of weight fraction, x_j (Equation 12), and weight percent , $\overline{x_j}$, (Equation 13).

$$E[C_{p,g}] = \sum_{j=1}^{j=n} E[x_j] E[C_{pj}] \tag{12}$$

$$E[C_{p,g}] = \frac{\sum_{j=1}^{j=n} E[\overline{x_j}] \cdot E[C_{pj}]}{\sum_{j=1}^{j=n} \overline{x_j}} \tag{13}$$

Similarly, the variance of $C_{p,g}$, denoted $V[C_{p,g}]$, can be written as the sum of the variances of the individual mineral contributions, $V[P_j]$.

$$V[C_{p,g}] = \sum_{j=1}^{j=n} V[P_j] \tag{14}$$

The variance of P_j is given by

$$V[P_j] = \left(\frac{\partial P_j}{\partial x_j}\right)^2 \cdot V[x_j] + \left(\frac{\partial P_j}{\partial C_{pj}}\right)^2 \cdot V[C_{pj}] \tag{15}$$

The partial derivatives in Equation (15) are evaluated using Equation (8) to give

$$V[P_j] = (E[C_{pj}])^2 \cdot V[x_j] + (E[x_j])^2 \cdot V[C_{pj}] \tag{16}$$

When mineral abundance is expressed as a weight fraction, (xj), Equation (17) is used to calculate the standard deviation for the rock-grain heat capacity, $\sigma[C_{p,g}]$. For mineral abundance expressed as weight percent, $\overline{x_j}$, Equation (18) is used:

$$\sigma[C_{p,g}] = \sqrt{\sum_{j=1}^{j=n} \left((E[C_{pj}] \cdot \sigma[x_j])^2 + (E[x_j] \cdot \sigma[C_{pj}])^2 \right)} \tag{17}$$

$$\sigma[C_{p,g}] = \frac{\sqrt{\sum_{j=1}^{j=n} \left((E[C_{p,g}] \cdot \sigma[\overline{x_j}])^2 + (E[\overline{x_j}] \cdot \sigma[C_{pj}])^2 \right)}}{\sum_{j=1}^{j=n} \overline{x_j}} \tag{18}$$

where the definition V[ ] = $(\sigma[\ ])^2$ has been employed. The standard deviations given by Equation (17) and (18) are with respect to the mean heat capacity over a selected temperature range.

If no temperature averaging is required only the uncertainties due to mineral abundance are considered in the rock-grain heat capacity determination. The resulting rock-grain heat capacity value is a function of temperature. For this case the mineral heat capacity is not uncertain, and Equations (12) and (13) are modified. The expected value of mineral heat capacity (i.e. $E[C_{pj}]$) is now replaced by a temperature dependent mineral heat capacity (i.e. $C_{pj}(T)$). Thus, the equation for the expected or average value of the rock-grain heat capacity as a function of mineral abundance expressed in terms of weight fraction, x_j (Equation 19), and weight percent , $\overline{x_j}$, (Equation 20):

$$E[C_{p,g}(T)] = \sum_{j=1}^{j=n} C_{pj}(T) \cdot E[x_j] \tag{19}$$

$$E[C_{p,g}(T)] = \frac{\sum_{j=1}^{j=n} C_{pj}(T) \cdot E[\overline{x_j}]}{\sum_{j=1}^{j=n} \overline{x_j}} \tag{20}$$

In determining the standard deviation of the rock-grain heat capacity for this case, the uncertainty in mineral heat capacity is not considered and thus results in the simplification of Equations (17) and (18). The standard deviation due to mineral heat capacity (i.e. $\sigma[C_{pj}]$) is zero and the expected value of mineral heat capacity (i.e. $E[C_{pj}]$) is replaced by a temperature

dependent mineral heat capacity (i.e. $C_{pj}(T)$). When mineral abundance is expressed as a weight fraction, (x_j), Equation (21) is used to calculate the standard deviation for the rock-grain heat capacity, $\sigma[C_{p,g}]$. For mineral abundance expressed as weight percent, $\overline{x_j}$, Equation (20) is used:

$$\sigma[C_{p,g}(T)] = \sqrt{\sum_{j=1}^{j=n} (C_{pj}(T) \cdot \sigma[x_j])^2} \tag{21}$$

$$\sigma[C_{p,g}(T)] = \frac{\sqrt{\sum_{j=1}^{j=n} (C_{pj}(T) \cdot \sigma[\overline{x_j}])^2}}{\sum_{j=1}^{j=n} \overline{x_j}} \tag{22}$$

4.2 Discussion of Results of the Rock-Grain Heat Capacity Calculations

The calculated average temperature dependent rock-grain heat capacity values for each selected stratigraphic unit, shown in Figures 4 and 5, are within acceptable range of heat capacities of similar rocks. The results show slightly higher heat capacities for units with high presence of zeolites. This is because clinoptilolite and mordenite, the sorptive zeolites with significant abundance, have higher heat capacity values (Figure 3). As described in Section 2 sorptive zeolites are significant in the Calico Hills formation layers and layers immediately above and below it. Thus in Figures 4 and 5, the Calico Hills layer Tac4 (Sequence 11) and the layer Tcplv-Tcpbt-Tcbuv (Sequence 7), located below the calico Hills, show the highest heat capacity values (See Table 2 for mineral abundances of these layers). The rest of the layers represented in Figure 4 show similar rock-grain heat capacity values because of their low mineral abundances of zeolites (sorptive and non-sorptive). At lower temperatures the PTn layer shows slightly higher rock-grain heat capacity values due to its relatively high abundance of volcanic glass. Figure 6 shows average temperature dependent rock-grain heat capacity for the layer Tptpll together with ± standard deviation. The standard deviation amounts to about 0.08 - 0.12 J/(g•K) in the specified temperature range. Examples of a combined mineral abundance and mineral heat capacity uncertainty values are discussed below.

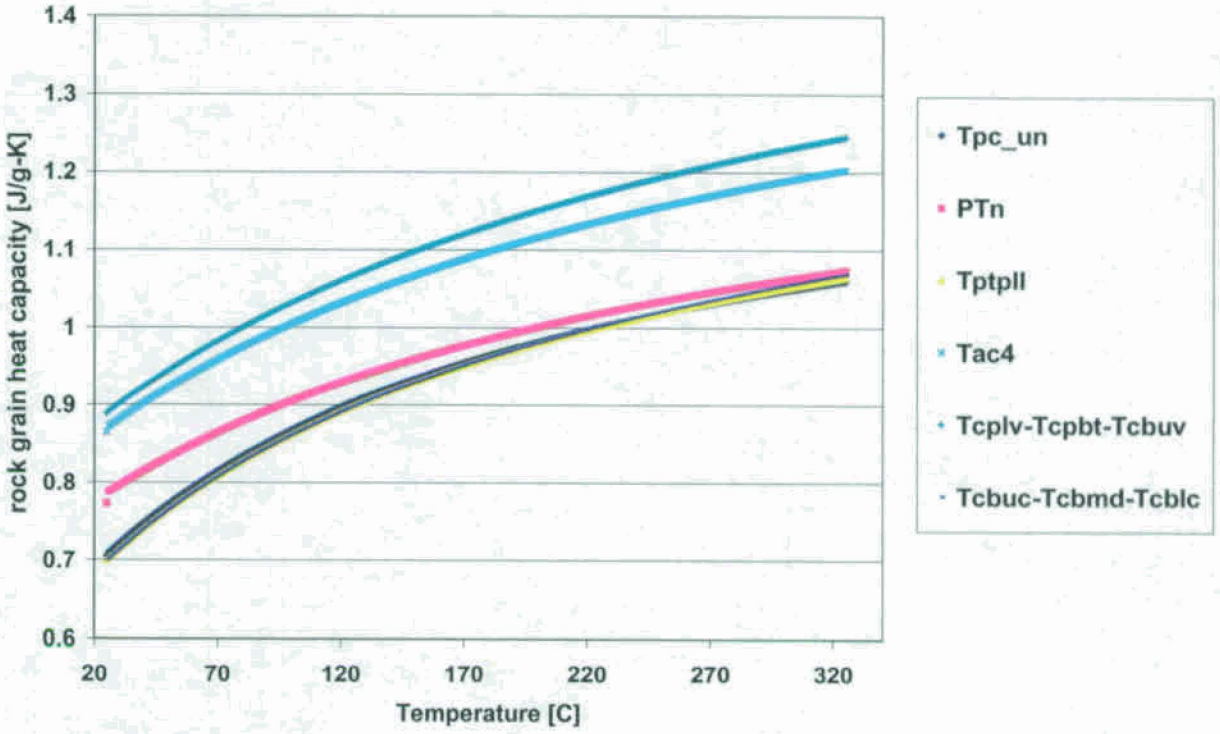

Figure 4. Average Rock Grain Heat Capacity of Selected Yucca Mountain Stratigraphic Layers

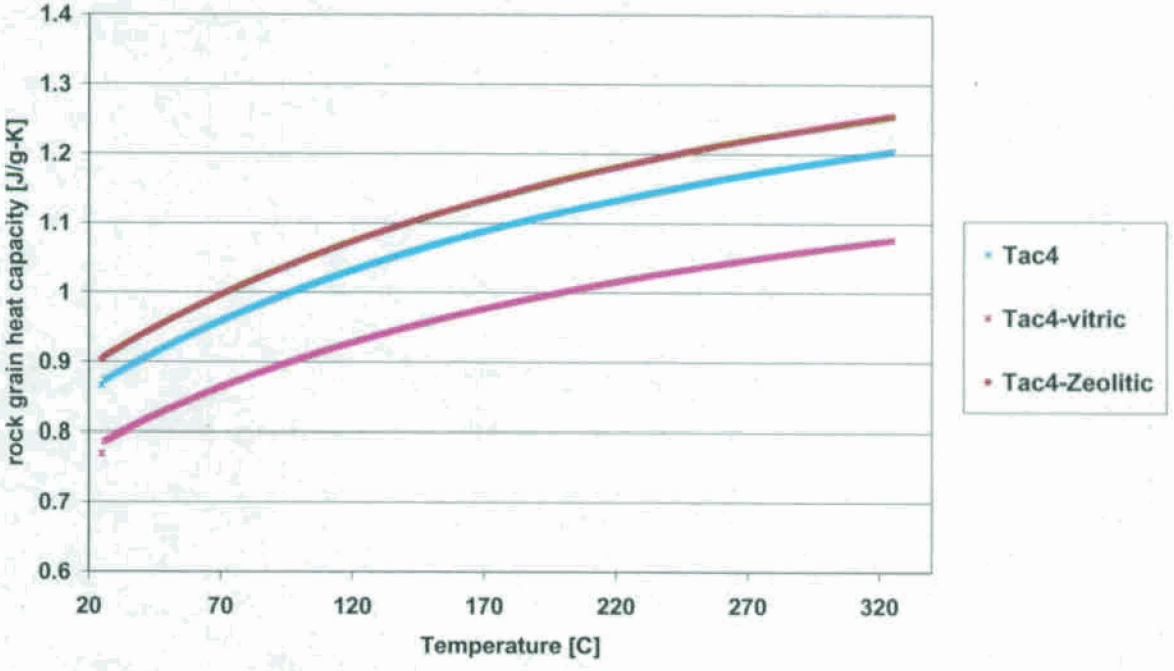

Figure 5. Average Rock Grain Heat Capacity of Selected Yucca Mountain Zeolitic and Vitric Calico Hills Formation Layers

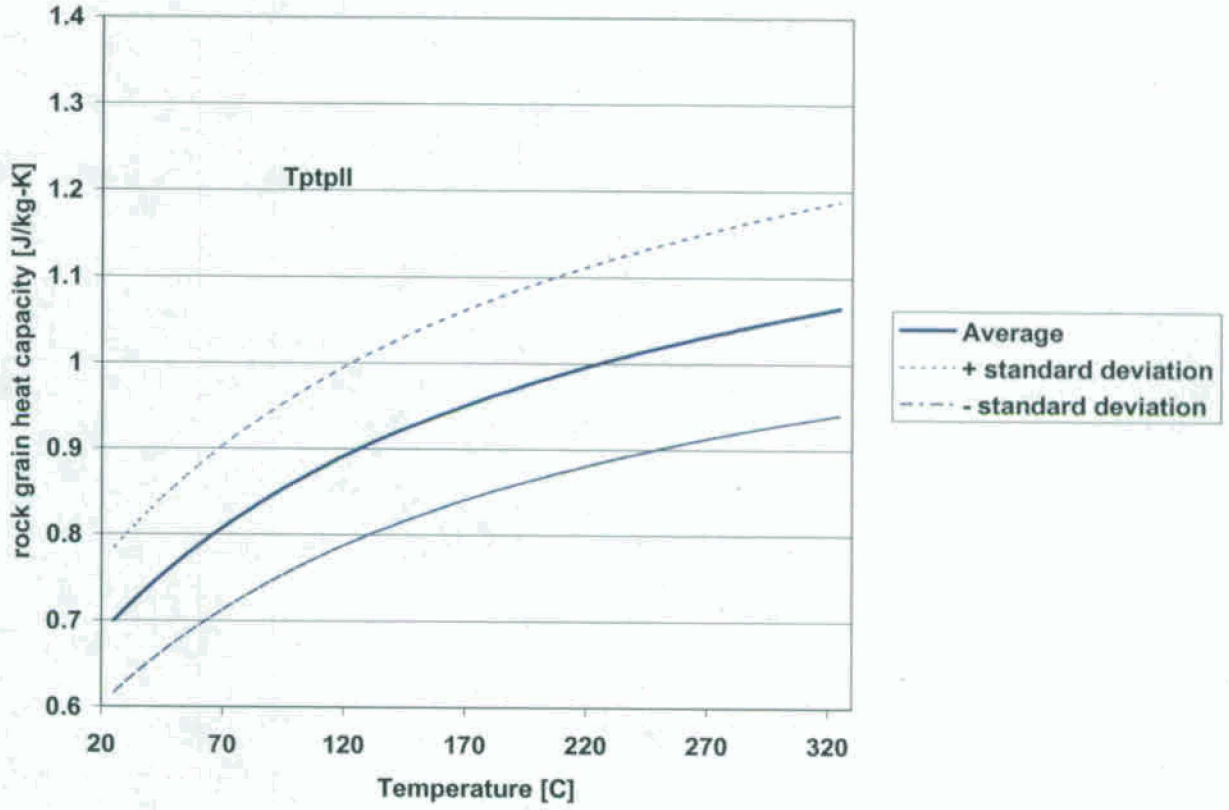

Figure 6. Average and standard deviation of Rock Grain Heat Capacity for the Stratigraphic Layer Tptpll

The rock-grain heat capacity values calculated using the mineral summation method have been compared with data from other sources. Comparison of the results developed in this report with those obtained using the oxide summation method of Nimick and Connolly (1991) are presented in Table 5. The calculated values for both methods represent the average value and associated uncertainty for two standard deviations for selected layers. Due to the different types of input data for the oxide summation data set the nomenclature for the layers varies. The horizontal lines in Table 5 denote the equivalent formation or layer to permit comparison of heat capacity values. Comparing the major element (oxide) data and the mineral summation data in Table 5 shows that the two methods give similar results for the average rock-grain heat capacity over the temperature range 25 °C to 325 °C. However, the estimates for standard deviation are, in general, higher for the mineral summation method when compared to the major element (oxide) method suggesting a little greater spread of the obtained heat capacity values. The higher standard deviation for the mineral summation method could be due to better accuracy in the measurement of oxide data in the major element (oxide) method. According to the Mineralogic Model (MM3.0) report (BSC 2004a) analytical uncertainty associated with the XRD analysis for mineral abundance can be higher in the case of lower mineral abundances.

Table 5: Comparison of Oxide and Mineral Summation Methods for Rock-Grain Heat Capacity

Based on major element oxide data			**Based on the mineral summation method (this work)**		
Model Layer	**Average Rock-grain heat capacity for T = 25 °C to 325 °C (J/g-K)**	**Two standard deviations of Rock-grain heat capacity (J/g-K)**	**Model layer**	**Average Rock-grain heat capacity for T = 25 °C to 325 °C (J/g-K)**	**Two standard deviations of Rock-grain heat capacity (J/g-K)**
Crystal Rich Tiva/Post-Tiva	0.985	0.202	Tpc_un	0.93	0.22
Tpbt4	1.040	0.254	PTn	0.96	0.46
Tptf	0.985	0.202	Tptpmn	0.93	0.28
Calico	1.038	0.176	Tac4	1.07	0.84
Prowmd	0.985	0.202	Tcplv-Tcbuv	1.10	0.38
Bullfroguv	1.040	0.254	Tcbuc-Tcblc	0.93	0.24

5. CONCLUSION

Average and standard deviations of rock-grain heat capacity values have been calculated for Yucca Mountain stratigraphic layers of the mineralogic model using the mineral summation method (utilizing Kopp's rule). The calculated rock-grain heat capacity values are valid over the temperature range of 25 °C to 325 °C. The calculation used mineral abundance and heat capacity data for ten mineral groups. The calculated rock-grain heat capacity is a strong function of temperature as shown in Figure 4. As discussed in Section 4.2 (and Table 5), the rock-grain heat capacity values compared very well to the rock-grain heat capacity values calculated using oxide summation data (Nimick and Connolly, 1991). This is important considering the uncertainty associated with the mineral abundance determination, variability in samples, and the collection of heat capacity data from different sources.

The rock-grain heat capacity equations are to be evaluated at different temperatures over the specified temperature range. When constant (i.e. temperature independent) values of rock-grain heat capacity are desired, the values can be averaged over the desired temperature range for the layer under consideration. The only exception to this is the heat capacity values of the Calico Hills formation and adjacent layers of bedded tuffs that are separated into vitric and zeolitic regions. For these layers separate constant rock-grain heat capacity values can be calculated for the vitric and zeolitic regions. In general, the developed values of heat capacity are appropriate because the layers are compositionally and mechanically homogenous. The limitations are that spatial variability has not been considered.

6. ACKNOWLEDGMENT

The authors would like to acknowledge the valuable contributions to this work provided by Yifeng Wang and Carlos Jove-Colon of Sandia National Laboratories. This work was supported by the Office of Repository Development as part of the Civilian Radioactive Waste Program, which is part of the Department of Energy. Sandia is a multiprogram laboratory operated by Sandia Corporation, a Lockheed Martin Company, for the United States Department of Energy under Contract DE-AC04-94AL85000.

7. REFERENCES

Berman, R.G. and Brown, T.H. 1985. "Heat Capacity of Minerals in the System Na2O-K2O-CaO-MgO-FeO-Fe2O3-Al2O3-SiO2-TiO2-H2O-CO2: Representation, Estimation, and High Temperature Extrapolation." *Contributions to Mineralogy and Petrology*, 89, 168-183. New York, New York: Springer-Verlag.

Berryman, James G. 1995. "Mixture Theories for Rock Properties." *AGU Reference Shelf3, RockPhysics and Phase Relations A Handbook of Physical Constants*. Ahrens, T.J. Pages 205-228. Washington, D.C.: American Geophysical Union.

BSC (Bechtel SAIC Company) 2004a. *Mineralogic Model (MM3.0) Report*. MDL-NBS-GS-000003 REV 01. Las Vegas, Nevada: Bechtel SAIC Company. ACC: DOC.20040908.0006.

BSC (Bechtel SAIC Company) 2004b. *Heat Capacity Analysis Report*. ANL-NBS-GS-000013 REV 01. Las Vegas, Nevada: Bechtel SAIC Company. ACC: DOC.20041101.0003.

BSC (Bechtel SAIC Company) 2004c. *Qualification of Thermodynamic Data for Geochemical Modeling of Mineral-Water Interactions in Dilute Systems*. ANL-WIS-GS-000003 REV 00. Las Vegas, Nevada: Bechtel SAIC Company. ACC: DOC.20041129.0006.

Buesch, D.C. and Spengler, R.W. 1999. "Correlations of Lithostratigraphic Features with Hydrogeologic Properties, a Facies-Based Approach to Model Development in Volcanic Rocks at Yucca Mountain, Nevada." *Proceedings of Conference on Status of Geologic Research and Mapping in Death Valley National Park, Las Vegas, Nevada, April 9-11, 1999*. Slate, J.L., ed. Open-File Report 99-153. Pages 62-64. Denver, Colorado: U.S. Geological Survey.

Buesch, D.C.; Spengler, R.W.; Moyer, T.C.; and Geslin, J.K.1996. *Proposed Stratigraphic Nomenclature and Macroscopic Identification of Lithostratigraphic Units of the Paintbrush Group Exposed at Yucca Mountain, Nevada.* Open-File Report 94-469. Denver, Colorado: U.S. Geological Survey.

Bulmer, M.G. 1979. *Principles of Statistics*. 3rd Edition. New York, New York: Dover.

Chipera, S.J.; Bish, D.L.; and Carlos, B.A. 1995. "Equilibrium Modeling of the Formation of Zeolites in Fractures at Yucca Mountain, Nevada." *Natural Zeolites '93: Occurrence, Properties, Use, Proceedings of the 4th International Conference on the Occurrence, Properties,*

and Utilization of Natural Zeolites, June 20-28, 1993, Boise, Idaho. Ming, D.W. and Mumpton, F.A., eds. Pages 565-577. Brockport, New York: International Committee on Natural Zeolites.

CRWMS (Civilian Radioactive Waste management System) M&O (Management and Operating Contractor) 1997. Determination of Available Volume for Repository Siting. BCA000000-01717-0200-00007 REV 00. Las Vegas, Nevada:

Deer, W.A.; Howie, R.A.; and Zussman, J. 1966. *An Introduction to the Rock-Forming Minerals.* New York, New York: John Wiley & Sons.

Dynamic Graphics, 2000. *Software Code*: EARTHVISION. V5.1, SGI/IRIX 6.5. 10174-5.1-00.

Flint, L.E. 1998. *Characterization of Hydrogeologic Units Using Matrix Properties, Yucca Mountain, Nevada.* Water-resources Investigations Report 97-4243. Denver Colorado: U.S. Geological Survey.

Johnson, G. K.; Flotow, H. E.; O'Hare, P.A.G.; and Wise, W.S. 1982. "Thermodynamic Studies of Zeolites: Analcime and Dehaydrated Analcime." *American Mineralogist*, 67, 736-748. Washington, D.C.: Mineralogical Society of America.

Klein, C. and Hurlbut, C.S., Jr. 1999. *Manual of Mineralogy.* 21st Edition, Revised. New York, New York: John Wiley & Sons.

Nimick, F.B. and Connolly, J.R. 1991. *Calculation of Heat Capacities for Tuffaceous Units from the Unsaturated Zone at Yucca Mountain, Nevada.* SAND88-3050. Albuquerque, New Mexico: Sandia National Laboratories. ACC: NNA.19910308.0017.

Peterman, Z.E. and Cloke, P.L. 2002. "Geochemistry of Rock Units at the Potential Repository Level, Yucca Mountain, Nevada with Erratum." *Applied Geochemistry*, 17, 683-698 and 955-958. New York, New York: Pergamon Press.

Robie, R.A. and Hemingway, B.S. 1995. *Thermodynamic Properties of Minerals and Related Substances at 298.15 K and 1 Bar (10 {superscript 5} Pascals) Pressure and at Higher Temperatures.* Bulletin 2131. Reston, Virginia: U.S. Geological Survey.

Robie, R.A.; Hemingway, B.S.; and Fisher, J.R. 1979. *Thermodynamic Properties of Minerals and Related Substances at 298.15 K and 1 Bar (10{superscript 5} Pascals) Pressure and at Higher Temperatures.* U.S. Geological Survey Bulletin 1452. Washington, D.C.: U.S. Government Printing Office.

Robinson, G.R., Jr. and Haas, J.L., Jr. 1983. "Heat Capacity, Relative Enthalpy, and Calorimetric Entropy of Silicate Minerals: An Empirical Method of Prediction." *American Mineralogist*, 68, 541-553. [Washington, D.C.: Mineralogical Society of America].

Thompson, A.B. and Wennemer, M. 1979. "Heat Capacities and Inversions in Tridymite, Cristobalite, and Tridymite-Cristobalite Mixed Phases." *American Mineralogist*, 64, 1018-1026. Washington, D.C.: Mineralogical Society of America.

APPENDIX A: HEAT CAPACITY SOURCES FOR THE TEN MINERAL GROUPS

For this study data from various sources have been used. Heat capacity data for the majority of the mineral groups (smectite, illite, cristobalite, quartz, feldspar, muscovite, and calcite) were obtained from BSC (2004c, Data Tracking Number: MO0009THRMODYN.001). The heat capacity data used for tridymite are from Robie et al. (1979, p. 218), and the heat capacity data for silica glasses are from Robie and Hemingway (1995, pp. 31 to 40, 50, and 58 to 66). Heat capacity data for chabazite, erionite, and stellerite used are from Chipera et al. (1995); heat capacity data for clinoptilolite and mordenite are from BSC (2004c, Data Tracking Number: MO0302SPATHDYN.001), and heat capacity data for analcime are from Johnston et al. (1982, p. 744, Equation 4). These data are summarized in BSC (2004b, Appendix A). A summary of the heat capacity data sources for the ten mineral groups and selection methods is given below.

A1. GROUP HEAT CAPACITY (SMECTITE + ILLITE)

Heat capacity data for smectite and illite were obtained from BSC (2004c, Data Tracking Number: MO0009THRMODYN.001). The heat capacities of smectite and illite are virtually the same. Above the water table the smectites typically have non-expandable illite contents of 10 to 20 percent. Well below the water table (depths greater than 1,000 meters or 3,300 feet below the surface), the ancient geothermal system generated abundant smectite and illite, but with a much higher illite content (80 to 90 percent) (BSC 2004a, Section 6.3.3). The primary area of interest for this study is above the water table. In addition, below the water table, the heat capacity behavior will be controlled by the fluid phase not the solid matrix material. Therefore, the heat capacity of the smectite-illite mineral group will be represented by smectite, due to their similar heat capacity values and because smectite is the dominant mineral above the water table.

A.2 GROUP HEAT CAPACITY FOR SORPTIVE ZEOLITES

Heat capacity data for chabazite, erionite, and stellerite are from Chipera et al. (1995); heat capacity data for clinoptilolite and mordenite are from BSC (2004c, Data Tracking Number: MO0302SPATHDYN.001). For this work the group heat capacity of sorptive zeolites was obtained by averaging the heat capacities of the individual members at specified temperatures. Heulandite is a fairly common mineral but its XRD abundance was combined with clinoptilolite because the two minerals have the same crystal structure (BSC 2004, p. 6-21). Because no XRD abundance of heulandite is available, its heat capacity was not included in the zeolite mineral group average. Due to the similar structure and chemical composition with clinoptilolite, not including heulandite in the average will have only a minor impact to the average zeolite mineral group heat capacity value.

A.3. TRIDYMITE

The heat capacity data for tridymite are from Robie et al. (1979, p. 218). Robie et al. (1979, p. 218) reported the heat capacity equation to be used within the given temperature limit. The temperature range for tridymite given by Robie et al. (1979, p. 218) is 117 °C to 1527 °C. They also give heat capacity data at 25 °C but did not provide data for temperatures in the range 25 °C to 117 °C (reported as uncertain). For this study, a straight-line interpolation was used to provide heat capacity for this temperature range. A straight-line interpolation was chosen because it is the simplest means of interpolating between two points (from 25 °C to 120 °C). By examination, the maximum difference in heat capacity between a fitted curve and linear interpolation over the

temperature range is approximately 0.25 to 0.30 J/g-K. The highest observed abundance of tridymite is approximately 10 percent. Therefore, it is estimated that the largest change in rock-grain heat capacity would be an increase of 0.03 J/g-K, which is well within the parameter uncertainty, and is deemed to be insignificant. Robie et al.'s equation was used for temperatures between 120 °C and 325 °C.

A.4 GROUP HEAT CAPACITY (CRISTOBALITE + OPAL-CT)

Heat capacity data for cristobalite was obtained from BSC (2004c, Data Tracking Number: MO0009THRMODYN.001). In terms of composition opal-CT is similar to quartz and tridymite. Opal-CT has a composition of (SiO_2 nH_2O), typically with a water of 4 to 9 percent and may be as high as 20 percent (Klein and Hurlbut, 1999, p. 531). Structurally, Opal-CT is a hydrous cryptocrystalline form of cristobalite, and is comprised of aggregates of cristobalite (Deer, et al., 1966, page 351). Plotting of heat capacity curves of compositionally similar minerals (cristobalite and quartz) shows that they are almost identical for temperatures below 250°C, with slight differences for temperatures between 250°C and 300°C BSC (2004b). Therefore it is assumed that the heat capacity of the cristobalite and Opal-CT mineral group can be represented by cristobalite.

A.5. QUARTZ

Heat capacity data for quartz was obtained from BSC (2004c, Data Tracking Number: MO0009THRMODYN.001).

A.6. FELDSPARS

Heat capacity data of feldspars was obtained from BSC (2004c, Data Tracking Number: MO009THRMODYN.001). Normative calculations based on major element analysis performed in the Yucca Mountain drift on samples from the repository horizon (Tptpul, Tptpmn, Tptpll, and Tptln) indicate that the feldspars throughout the sequence would likely be alkali feldspars (Peterman and Cloke, Table 5, 2002). Because of their identical structure and similar composition (Na-K solid solution series from albite to orthoclase), the heat capacity for K-feldspar can be used to represent Yucca Mountain feldspars.

A.7. VOLCANIC GLASS

Heat capacity data for volcanic glasses were obtained from Robie and Hemingway (1995). The heat capacity of volcanic glass was approximated by an average value based on the following glass compositions.

$Ca_3Al_2Si_3O_{12}$, $Mg_3Al_2Si_3O_{12}$, $(Mg_{1.5}Ca_{1.5})Al_2Si_3O_{12}$, $CaSiO_3$, $CaAl_2SiO_6$, $CaFeSi_2O_6$,, $CaMgSi_2O_6$, $MgSiO_3$, $NaAlSi_2O_6$, $KAlSi_3O_8$, $NaAlSi_3O_8$, $NaAlSiO_4$

A.8. NONSORPTOVE ZEOLITE (ANALCIME)

Heat capacity data for analcime was obtained from Johnson et al. (1982, p. 744, Equation 4)

A.9. MUSCOVITE

The heat capacity for muscovite was obtained from BSC (2004c, Data Tracking Number: MO0009THRMODYN.001). Structurally biotite and muscovite are both sheet silicates, and, compositionally, they very similar (biotite is Fe rich and muscovite is Al rich (Deer et. al., 1966, pp. 201 and 211)). Because of their similar structure, the heat capacity of muscovite can be use to represent mica.

A.10. CALCITE

The heat capacity for calcite was obtained from BSC (2004c, Data Tracking Number: MO0009THRMODYN.001).